Supporting information for

Protein-induced modifications in crystal morphology of a hydrogen-bonded organic framework

Kate L. Flint,[a] Jack D. Evans,[a] Francesco Carraro,[b] Simon Renner,[b] Oliver M. Linder-Patton,[a] Heinz Amenitsch,[c] Robert J. Falconer,[d] Nicholas G. White,[e] Christopher J. Sumby,*[a] Paolo Falcaro*[b] and Christian J. Doonan*[a]

a. Department of Chemistry, School of Physics, Chemistry and Earth Sciences, The University of Adelaide, Adelaide, SA 5005, Australia. Email: christopher.sumby@adelaide.edu.au; christian.doonan@adelaide.edu.au

b. Institute of Physical and Theoretical Chemistry, Graz University of Technology, Stremayrgasse 9, Graz 8010, Austria. Email: paolo.falcaro@tugraz.at

c. Institute for Inorganic Chemistry, Graz University of Technology, Stremayrgasse 9, Graz 8010, Austria

d. School of Chemical Engineering, The University of Adelaide, Adelaide, SA 5005, Australia.

e. Research School of Chemistry, The Australian National University, Canberra, ACT 2601, Australia.

S1 Experimental

Materials. Lysozyme was purchased from Astral Scientific, and all other proteins were purchased from Sigma-Aldrich. Each of the proteins tested was a lyophilised powder; proteins were used without further purification. *N*-(3-dimethylaminopropyl)-*N'*-ethylcarbodiimide hydrochloride (EDC.HCl) was purchased from Sigma-Aldrich, acetic anhydride from Chem Supply, and ethylene diamine (EDA) from Merck. 4,4',4'',4'''-Methanetetrayltetrabenzimidamide tetrahydrochloride (**1**·Cl_4), and the potassium salt of azobenzene-4,4'-dicarboxylic acid (**2**) were prepared as previously described.[1,2] The water used was ultra-pure Milli-Q (MQ) with resistivity of 18 MΩ cm^{-1} (Merck Millipore Milli-Q IQ 7000 Ultrapure Lab Water System purification system). All other buffers and solvents were purchased from commercial sources and used without further purification.

S1.2 Protein surface modifications

Acetylation reaction. The method for the acetylation of proteins was adapted from literature procedures.[3] BSA (20 mg) was dissolved in 4 mL phosphate buffer (PB, 100 mM, pH 8). A 50-fold molar excess of acetic anhydride was added in small increments over 1 hour. The pH was adjusted back to pH 8 using 2 M NaOH after each addition and the solution stirred for 1 hour after the final addition. The protein solution was washed by ultrafiltration once with PB (100 mM, pH 7.4) and twice with MQ water to remove excess salts (Microsep™ Advance Centrifugal Device, 10 kDa at 4000 rpm/1699 *g*). The protein solution was concentrated to approximately 4 mg mL^{-1} in MQ water.

Amination reaction. The method for the chemical amination was adapted from a literature procedure.[3] A 2 mL solution of EDA (0.268 mL, 4.01 mmol) in MQ water was prepared and the pH was adjusted to 4.5 using 6 M HCl. The protein (20 mg, BSA) was added, followed by EDC.HCl (7.2 mg, 0.038 mmol). The solution was stirred on ice for 120 minutes. The protein solution was washed by ultrafiltration once with PB (100 mM, pH 7.4) and twice with MQ water to remove excess salts (Microsep™ Advance Centrifugal Device, 10 kDa at 4000 rpm/1699 *g*). The protein solution was concentrated to approximately 4 mg mL^{-1} in MQ water.

Fluorescein tagged proteins. BSA (40 mg) and fluorescein isothiocyanate (FITC) (0.5 mg) were dissolved in carbonate-bicarbonate buffer (0.1 M, pH 9.2, 4 mL) and left for 2 h in darkness at room temperature under gentle stirring. The FITC-tagged BSA (F-BSA) was recovered by passing the reaction mixture through a NAP-25 column (GE Healthcare Life Sciences, NSW, Australia). The crude F-BSA solution was concentrated and exchanged into ultra-pure water using a 10 K membrane by centrifugation (1699 *g*, 3 x 20 mins). The F-BSA was stored in darkness at 4°C prior to use.

S1.3 Biocomposite syntheses

HOF protein-free synthesis. HOF synthesis was adapted from literature procedures.[4] Aqueous solutions of **1**.Cl_4 (5 mL) and K_2.**2** (5 mL) were mixed and left undisturbed for 24 hours. The resulting precipitate recovered by centrifugation (2000 *g*, 10 minutes), and washed twice with water.

For samples synthesised from *cis*-K_2.**2**, a solution of K_2.**2** (5 mL) was first exposed to UV-light (365 nm, 100 W, 2 h) before addition to **1**.Cl_4 (5 mL).

For samples synthesised at reduced temperature, aqueous solutions of **1**.Cl_4 (5 mL) were first cooled in the refrigerator, before the addition of K_2.**2** (5 mL). Solutions of *trans*-K_2.**2** were pre-chilled in the refrigerator prior to addition, and solutions of *cis*-K_2.**2** were cooled on ice immediately after irradiation.

Protein@HOF synthesis. A similar method was used for protein encapsulation, where a protein (0.03 µmol) was dissolved in an aqueous solution of **1**.Cl_4 (5 mL), before addition of K_2.**2** (5 mL).

Adjustments to ligand concentration. The overall concentrations of ligand precursors were adjusted according to Table S1. Protein quantities and total volume remained constant.

Table S1: Ligand equivalents for synthesis of HOF

	K_2.**2**	**1**.Cl_4
HIGH (500 : 1)	2 mM, 5 mL (3.46 mg, 10 µmol)	1 mM, 5 mL (3.16 mg, 5 µmol)
MEDIUM (250 : 1)	1 mM, 5 mL (1.73 mg, 5 µmol)	0.5 mM, 5 mL (1.58 mg, 2.5 µmol)
LOW (75 : 1)	0.3 mM, 5 mL (0.525 mg, 1.5 µmol)	0.15 mM, 5 mL (0.474 mg, 0.75 µmol)

Photoswitching of K_2.2. The *trans-cis* isomerisation of K_2.**2** was first assessed by monitoring the isomer distribution by ^{1}H NMR spectroscopy. Before irradiation the sample was predominantly the *trans* form (> 90%). Immediately following UV irradiation (365 nm, 100 W, 2 h) 64% was found to have been isomerised to the *cis* form, in good agreement with the photoswitching reported for this ligand by White and coworkers.[4] The percentage of *cis*-**2** was measured at different time intervals after exposure by comparing the integrations of *trans*-**2** and *cis*-**2** peaks, and these data used to plot the isomerisation of the *cis* form back to the *trans* form.

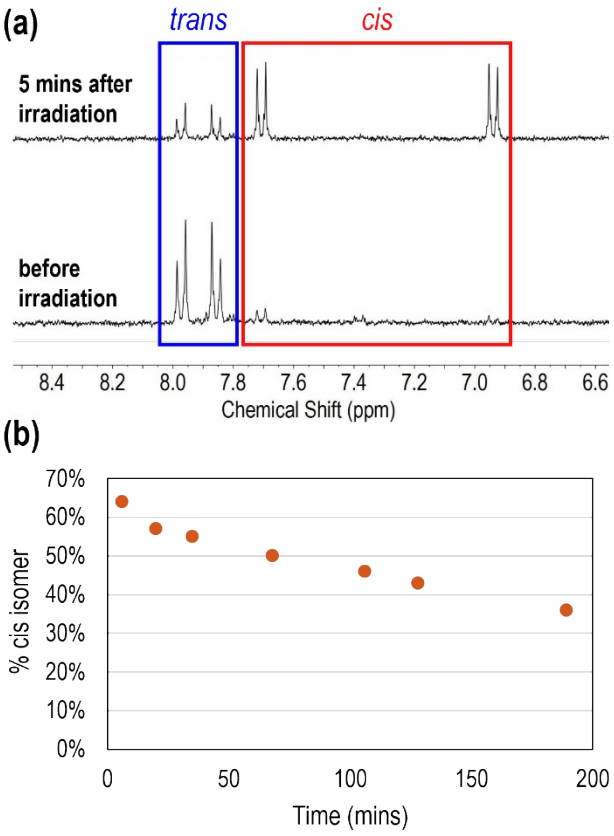

*Figure S1: (a) Stacked truncated ^{1}H NMR spectra of K_2.**2** dissolved in D_2O before and after irradiation with 365 nm light (0.50 mM in D_2O, 300 MHz, 298 K); (b) percentage of cis-**2** at different time intervals after irradiation with 365 nm light.*

S1.4 Characterisation

Powder X-ray diffraction (PXRD). PXRD data were collected on a Bruker D4-Endeavor diffractometer (flat plate) using a Co Kα (λ=1.78897 Å) radiation source. Data was collected over the range 2θ of 2° to 50° and was expressed as Cu radiation using Pow DLL converter (version 2.68.00). Simulated powder X-ray diffraction patterns were generated from the single crystal X-ray data using Mercury.[5]

Scanning electron microscopy (SEM). SEM images were collected using a Hitachi SU7000 Ultra-High Resolution scanning electron microscope or a Quanta 450 Field Emission Scanning Electron Microscope. Prior to analysis the samples were dry-loaded or dispersed in water and drop-cast onto an adhesive carbon tab on a 12 mm aluminium SEM stage, and sputter-coated with a 5 mm platinum thin film.

UV/Visible analysis (UV/Vis). Spectra were recorded at 25 °C on an Agilent Cary UV/Vis Compact spectrophotometer.

Zeta potential measurements. Zeta potentials of proteins were obtained using folded capillary zeta cells (DTS1070). Proteins were dissolved to a concentration of ~1 mg/mL – 5 mg/mL in 10 mM KCl and passed through a 0.2 µm syringe filter prior to analysis. Measurements were performed in triplicate, with each measurement consisting of 30 runs with a 120 s prior incubation period. The following measurement parameters were used: Temperature = 25.0 °C, material RI =

1.450, dispersant RI = 1.330, dispersant viscosity = 0.8854 cP, dispersant dielectric constant = 78.5, f(Ka) = 1.5 (Smoluchowski approximation).

Confocal laser scanning microscopy (CLSM). CLSM images were taken on an Olympus FV3000 confocal laser scanning microscope. The samples were excited at 488 nm, and the fluorescence signal was collected between 495 - 545 nm.

Isothermal titration calorimetry (ITC). Calorimetric analysis was conducted using a MicroCal PEAQ-ITC (Malvern Panalytical) set at 298, 308, 313, or 318 K. Lysozyme and BSA were washed by ultrafiltration with Tris-HCl buffer (10 mM, pH 7.4) (Microsep™ Advance Centrifugal Device, 10 kDa at 4000 rpm/1699 *g*) and prepared to a concentration of 1 mM in Tris-HCl buffer (10 mM, pH 7.4). HOF particles were prepared to 2 mg/mL in Tris-HCl buffer (10 mM, pH 7.4). The injection syringe contained 1 mM protein which was titrated into the sample cell, which contained the HOF particle solution. An initial 0.4 µL injection, followed by 14 x 2.5 µL injections of 1 mM protein into 2 mg/mL HOF particles, were made over the course of the titration. In each titration the reference cell contained water. The time delay between each injection was 150 seconds, and the RPM (rotations per minute) was set to 750 to ensure thorough mixing of the cell. Data analysis was performed using the MicroCal PEAQ-ITC analysis software (Malvern Panalytical). The enthalpy of dilution of protein was subtracted from the raw data. The first injection of 0.4 µL was used to prime the needle and although included in the data, should be disregarded.

Nuclear magnetic resonance spectroscopy (NMR). All ^{1}H NMR spectra were obtained using a Bruker Ascend 300 operating at 25°C.

S2 Protein surface modification data

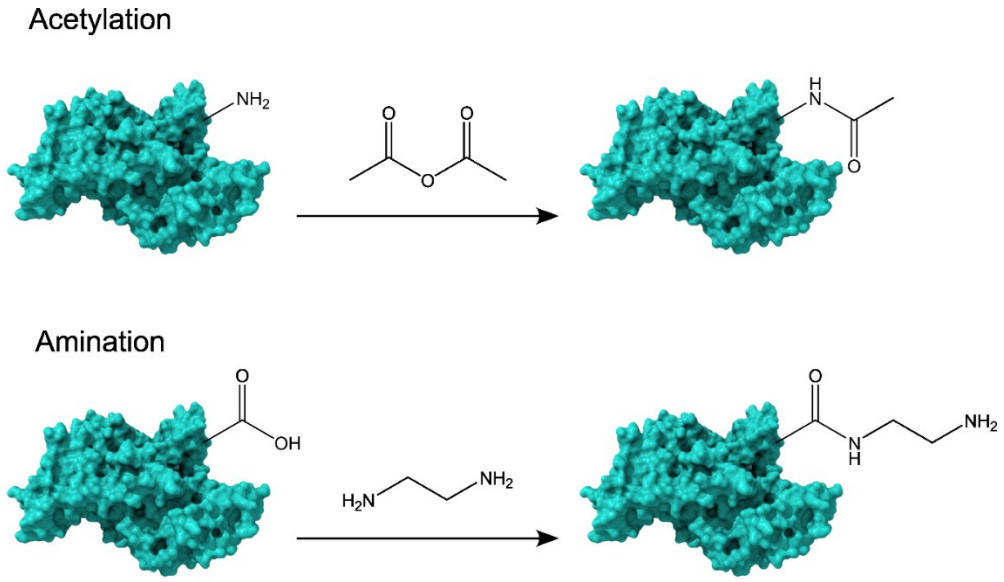

Figure S2: Surface modification reactions. Acetylation lowers the pI of a protein by modification of the exposed amine groups. Amination raises the pI of a protein by capping carboxyl groups with a free amine.

Table S2: Experimental zeta potential in a 10 mM KCl solution, and binary crystal deformation result for each protein tested in this work. The yes/no descriptor for crystal deformation indicates whether extensive alteration to HOF crystal morphology (compared to samples containing no protein) was observed by SEM imaging.

Protein	Size (kDa)	Zeta Potential (mV)	Crystal Deformation?	Modification	Zeta Potential (mV)	Crystal Deformation?
BSA	66.5	-11.3 ± 3.28	Yes	Acetylation Amination	-35.7 ± 1.58 10.5 ± 1.82	Yes Yes
HRP	44	-8.08 ± 0.939	Yes			
Urease	550	-9.35 ± 1.35	Yes			
Lipase B	33	-19.0 ± 1.01	No			
Lysozyme	14.3	12.0 ± 1.75	No			
Myoglobin	17	-9.34 ± 1.70	No			

S3 Time course crystal growth studies

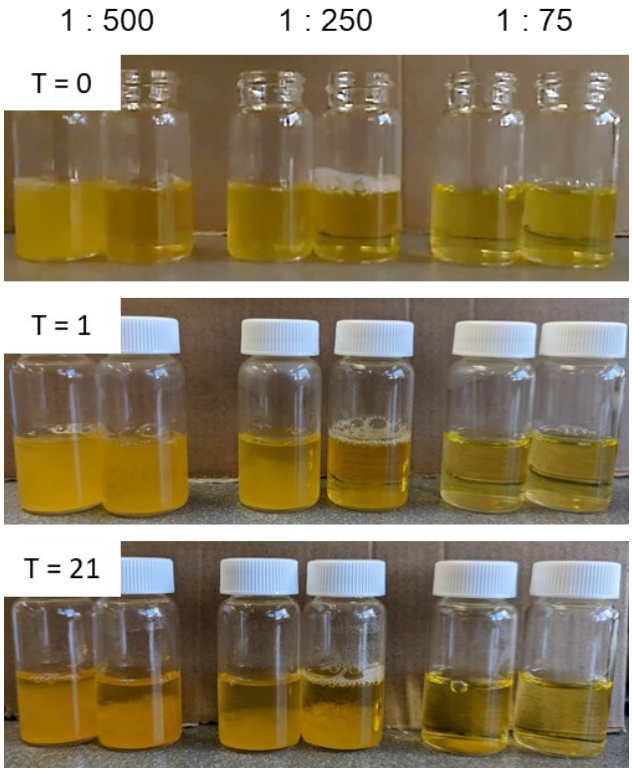

*Figure S3: Sequential photographs of **Bovine Serum Albumin (BSA)** samples immediately after mixing of the ligand solutions (T = 0), after 1 hour (T = 1), and after 21 hours (T = 21). The three ratios of protein to total ligand are shown (1 : 500, 1 : 250, 1 : 75), and both forms of K_2.**2** were used within each sample pair (left = trans, right = cis). The trans ligand forms show faster crystal formation than samples where the cis ligand was added, which remain clear immediately after ligand addition.*

S4 Powder X-ray diffraction (PXRD) data

Unless otherwise stated, samples were suspended overnight in MQ water, drop cast onto silicon wafers, and left to slowly evaporate over the course of 3 – 5 hours, before data collection. Evaporation time was dependent on the quantity of sample present and particle size, with complete air drying resulting in loss of crystallinity.

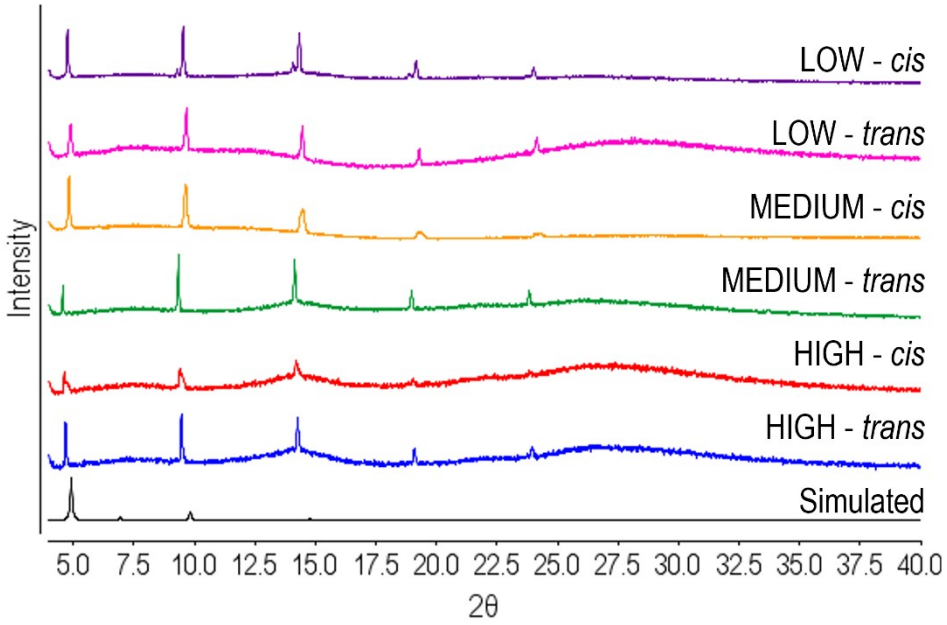

Figure S4: Power X-ray diffraction patterns of HOF samples at three different ligand concentrations in the absence of protein. Data collected using solvated samples with minimal H_2O present.

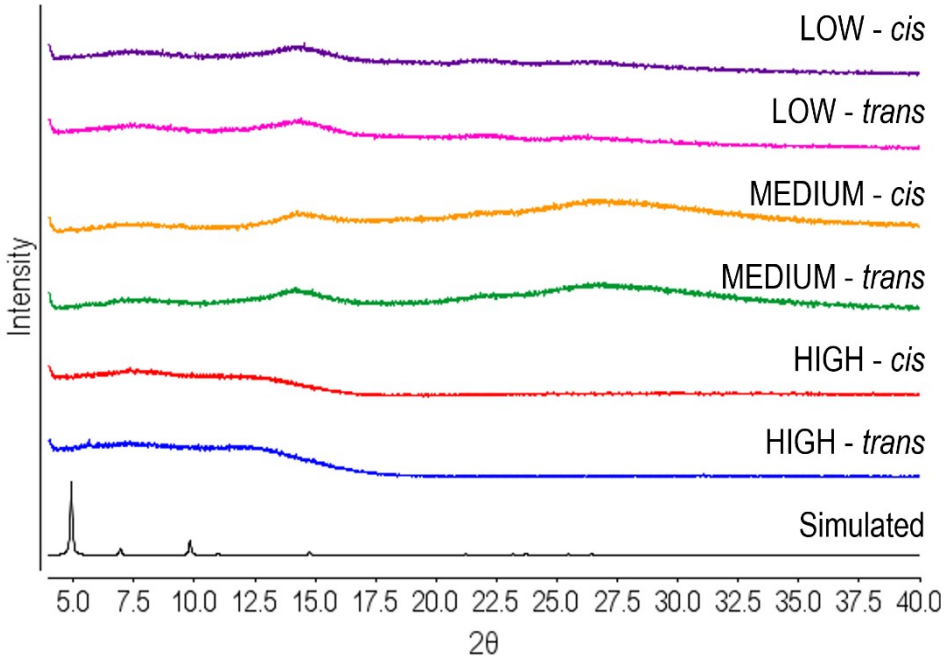

*Figure S5: Power X-ray diffraction patterns of dried HOF samples at three different ligand concentrations in the presence of **Bovine Serum Albumin (BSA)**. Samples were drop cast onto silicon wafers and allowed to evaporate to dryness.*

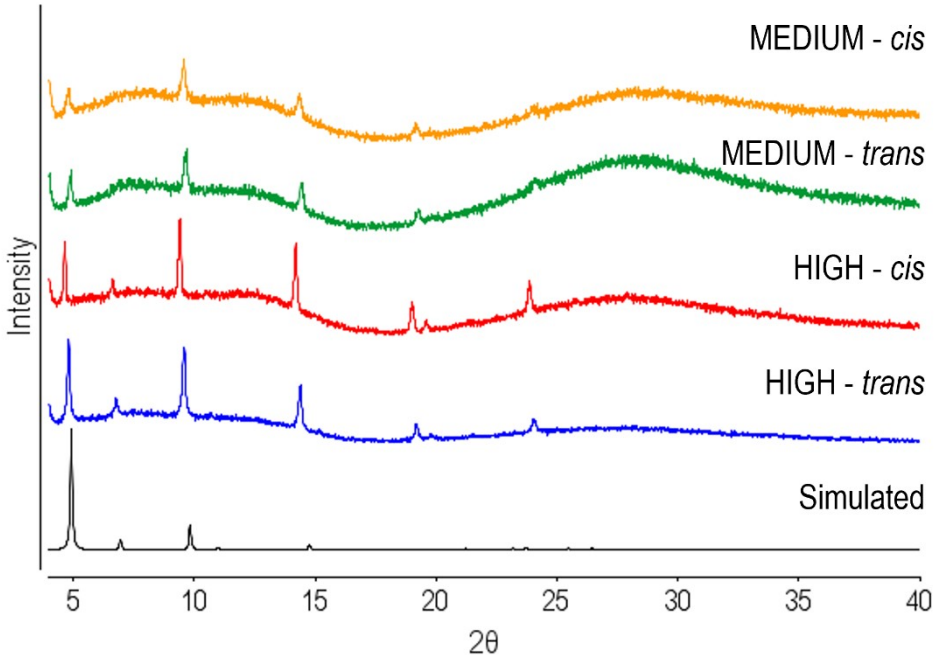

Figure S6: Power X-ray diffraction patterns of hydrated HOF samples at three different ligand concentrations in the presence of ***Bovine Serum Albumin (BSA)****. Conditions for resuscitation were unable to be found for LOW – cis, and LOW – trans samples.*

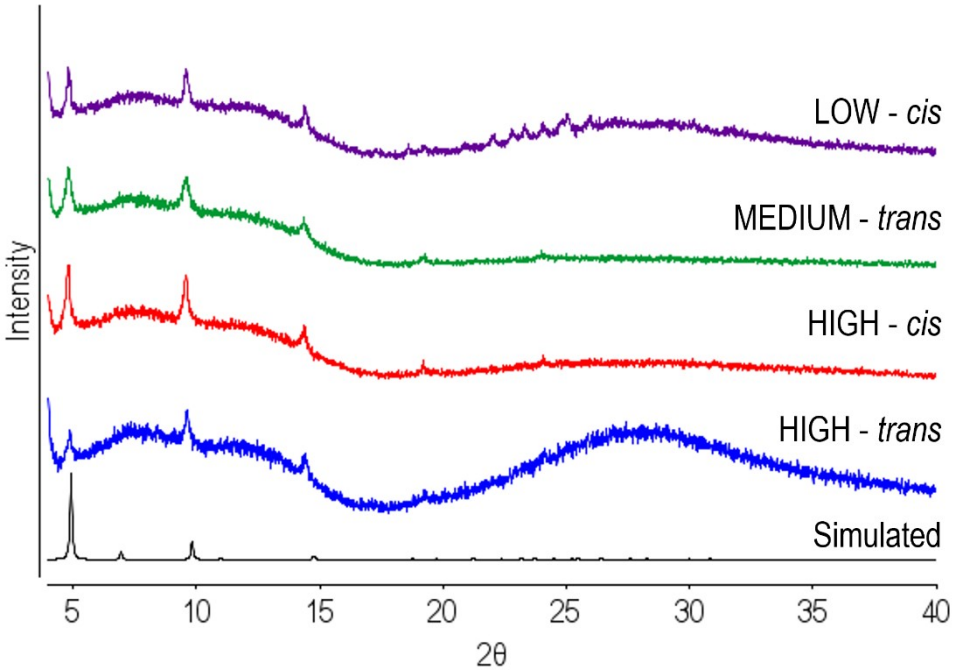

Figure S7: Power X-ray diffraction patterns of hydrated HOF samples at three different ligand concentrations in the presence of ***Horseradish Peroxidase (HRP)****. Conditions for resuscitation were unable to be found for MEDIUM – cis, and LOW – trans samples.*

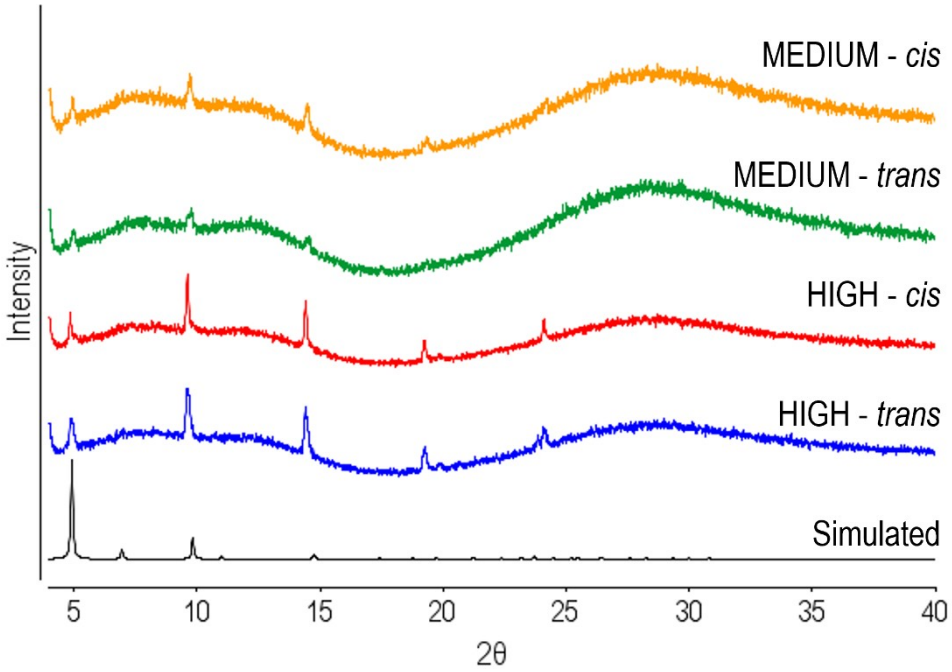

Figure S8: Power X-ray diffraction patterns of hydrated HOF samples at three different ligand concentrations in the presence of ***Urease****. Conditions for resuscitation were unable to be found for LOW – cis, and LOW – trans samples.*

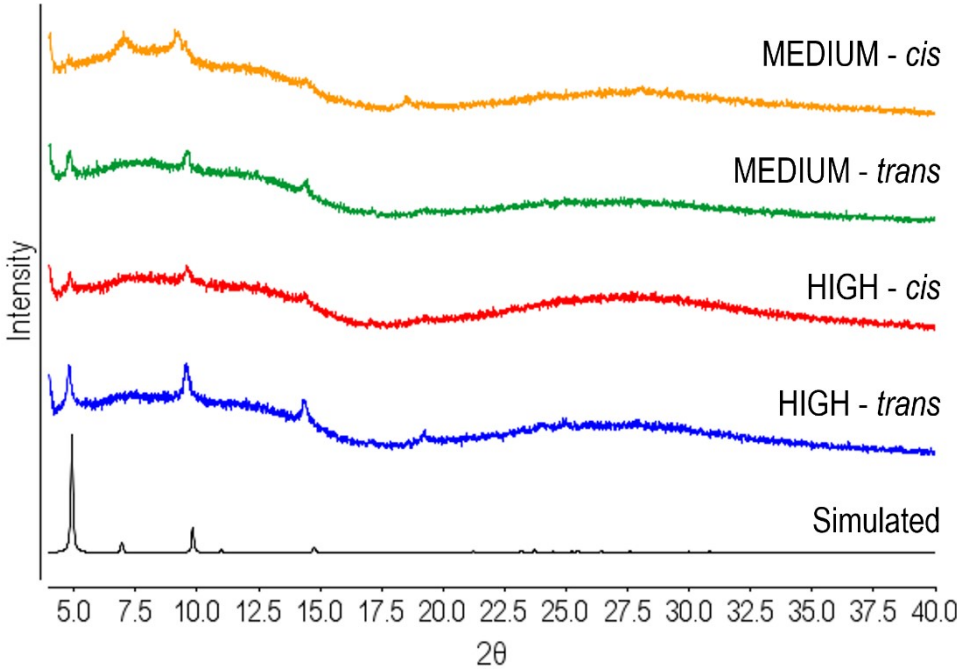

Figure S9: Power X-ray diffraction patterns of hydrated HOF samples at three different ligand concentrations in the presence of ***Lysozyme****. Conditions for resuscitation were unable to be found for LOW – cis, and LOW – trans samples.*

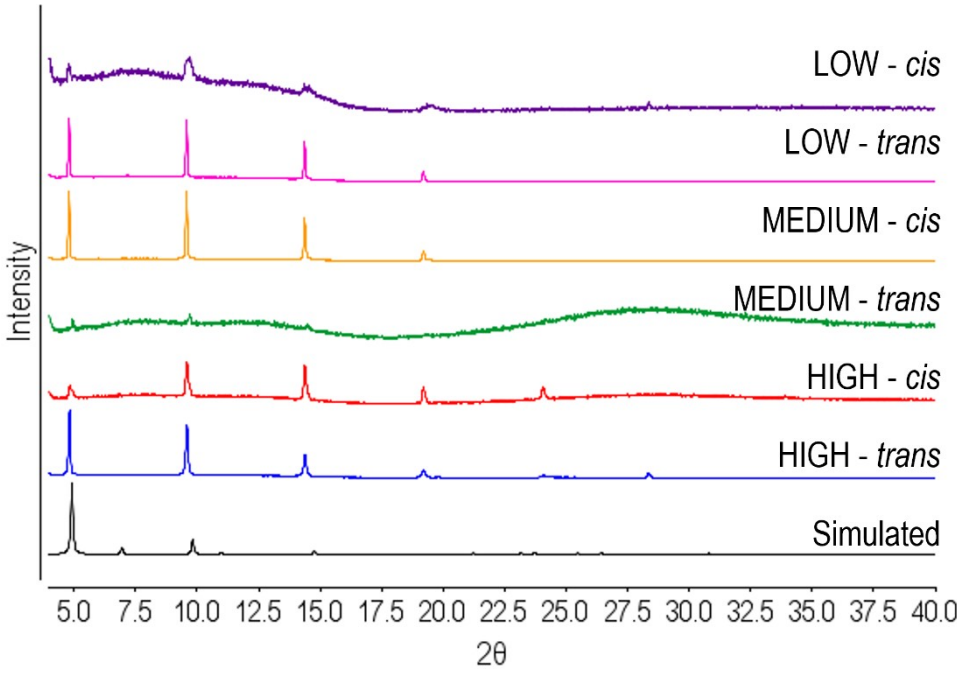

Figure S10: Power X-ray diffraction patterns of hydrated HOF samples at three different ligand concentrations in the presence of ***Myoglobin****.*

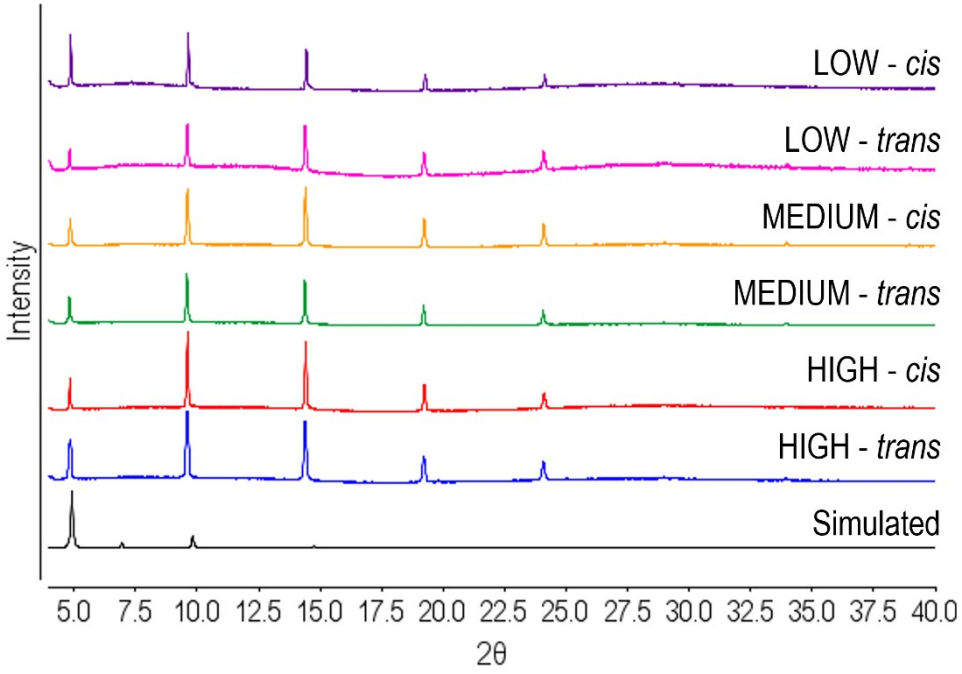

Figure S11: Power X-ray diffraction patterns of hydrated HOF samples at three different ligand concentrations in the presence of ***Lipase B from Candida Antarctica (CALB)****.*

S5 Scanning electron microscopy

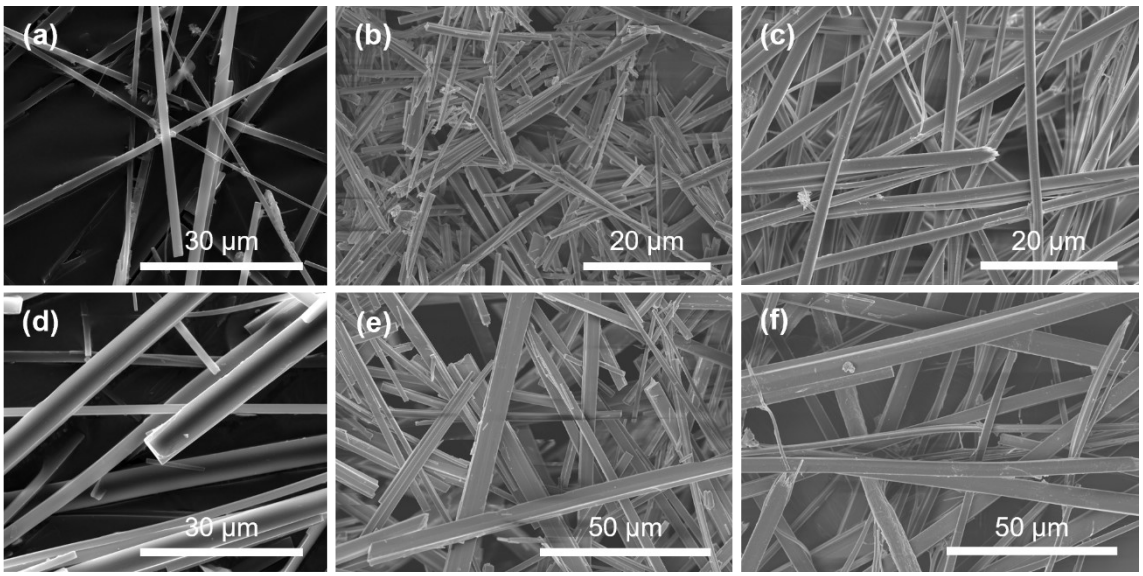

*Figure S12: SEM images of HOF grown in the absence of protein, showing crystals grown upon addition of the (a, b, c) trans- and (d, e, f) cis-K_2.**2** ligand, at HIGH, MEDIUM, and LOW total ligand concentration (L → R).*

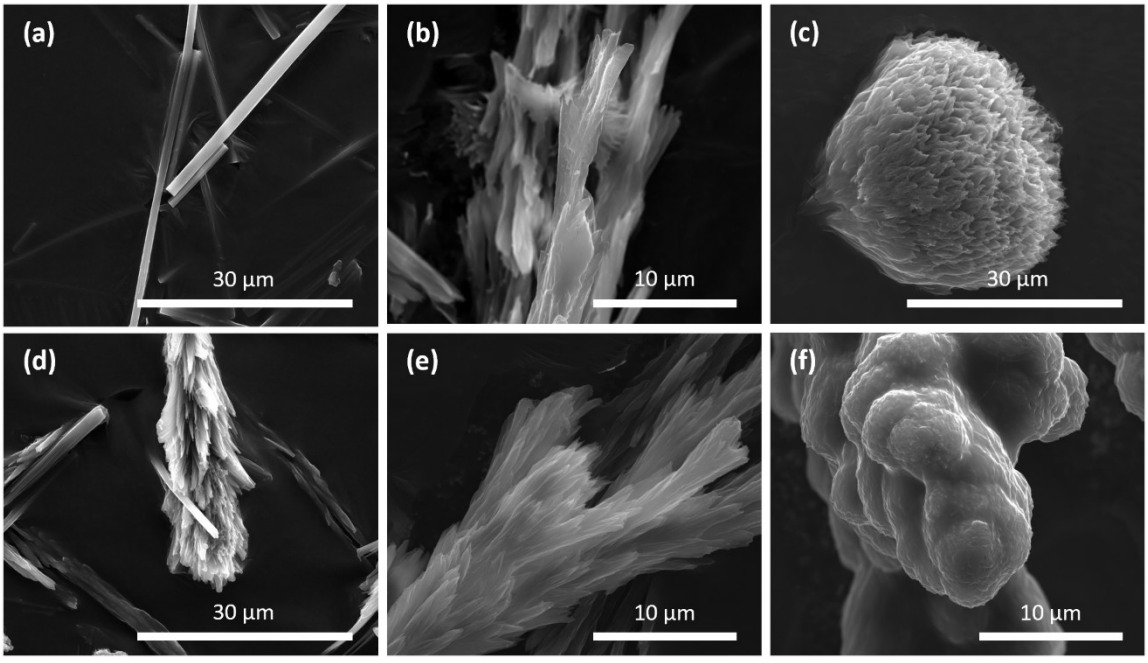

*Figure S13: SEM images of HOF grown in the presence of **BSA**, showing crystals grown upon addition of the (a, b, c) trans- and (d, e, f) cis-K_2.**2** ligand, at HIGH, MEDIUM, and LOW total ligand concentration (L → R).*

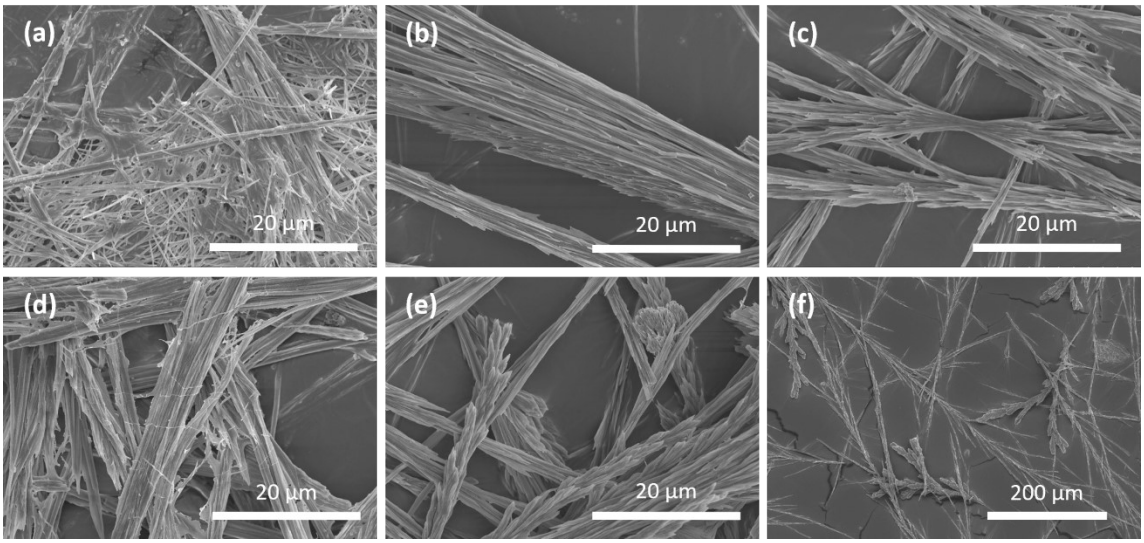

*Figure S14: SEM images of HOF grown at reduced temperature (4°C) in the presence of **BSA**, showing crystals grown upon addition of the (a, b, c) trans- and (d, e, f) cis-K_2.**2** ligand at HIGH, MEDIUM, and LOW total ligand concentration (L → R).*

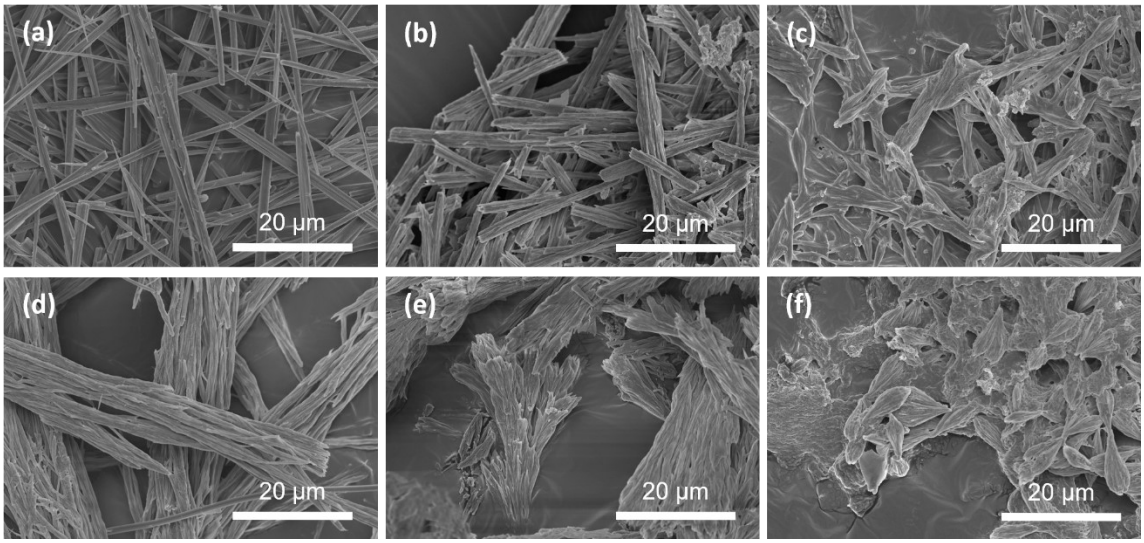

*Figure S15: SEM images of HOF grown in the presence of **acetylated BSA**, showing crystals grown upon addition of the (a, b, c) trans- and (d, e, f) cis-K_2.**2** ligand, at HIGH, MEDIUM, and LOW total ligand concentration (L → R).*

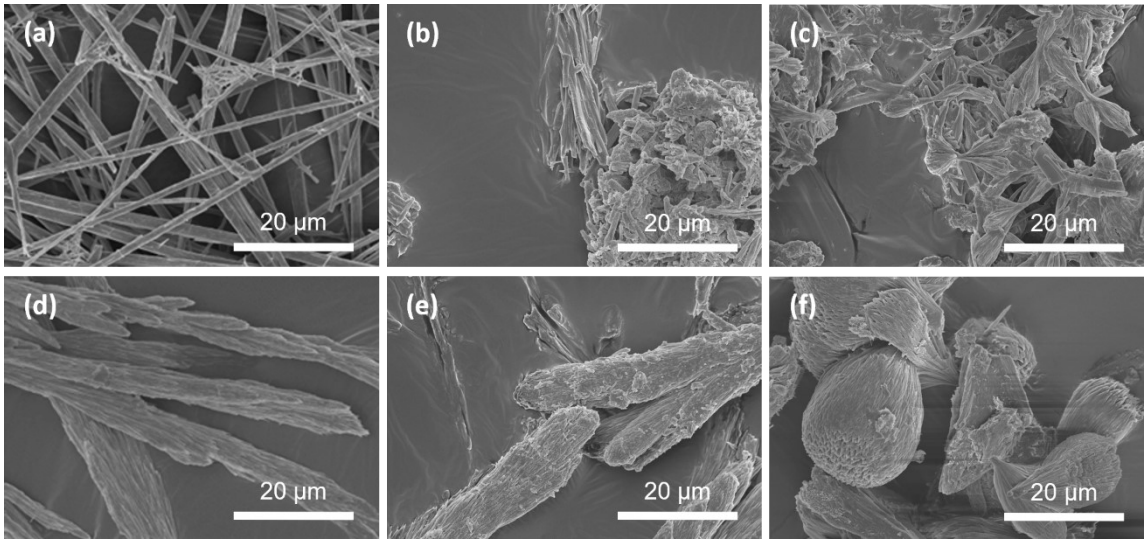

*Figure S16: SEM images of HOF grown in the presence of **aminated BSA**, showing crystals grown upon addition of the (a, b, c) trans- and (d, e, f) cis-K_2.**2** ligand, at HIGH, MEDIUM, and LOW total ligand concentration (L → R).*

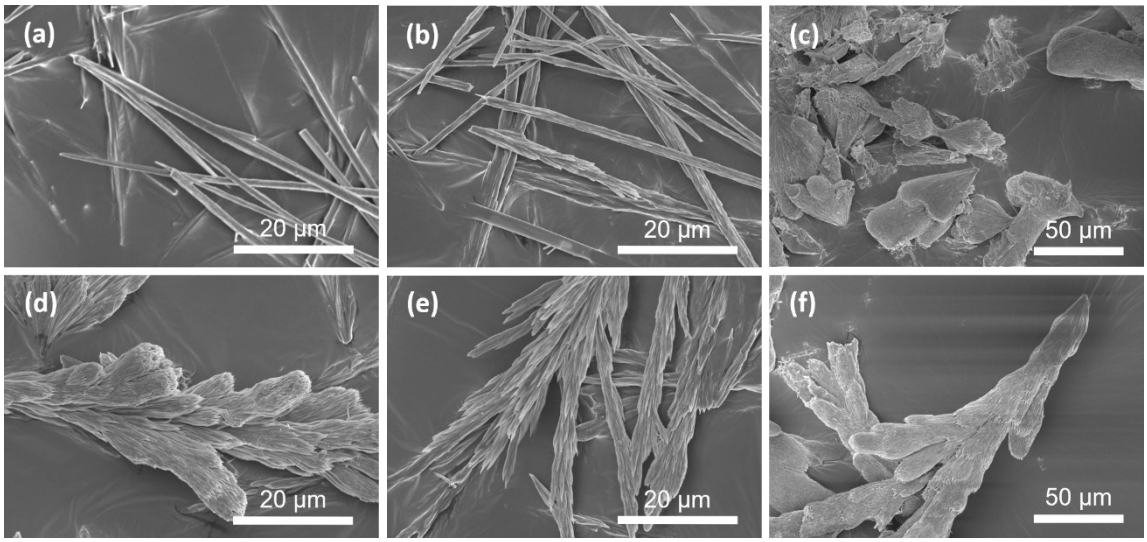

*Figure S17: SEM images of HOF grown in the presence of **HRP**, showing crystals grown upon addition of the (a, b, c) trans- and (d, e, f) cis-K_2.**2** ligand, at HIGH, MEDIUM, and LOW total ligand concentration (L → R).*

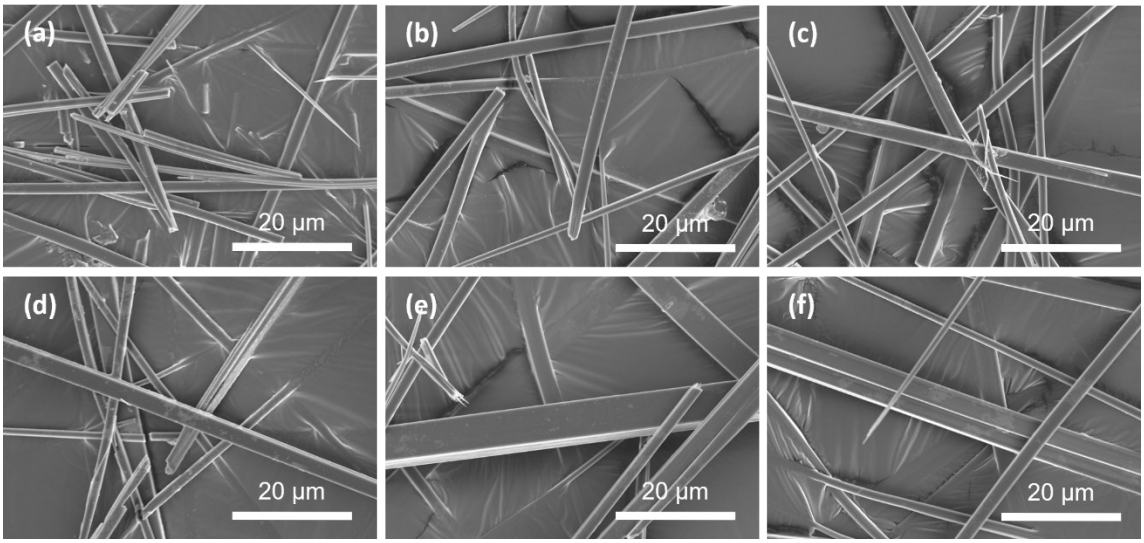

*Figure S18: SEM images of HOF grown in the presence of **Lipase B from Candida Antarctica**, showing crystals grown upon addition of the (a, b, c) trans- and (d, e, f) cis-K_2.**2** ligand, at HIGH, MEDIUM, and LOW total ligand concentration (L → R).*

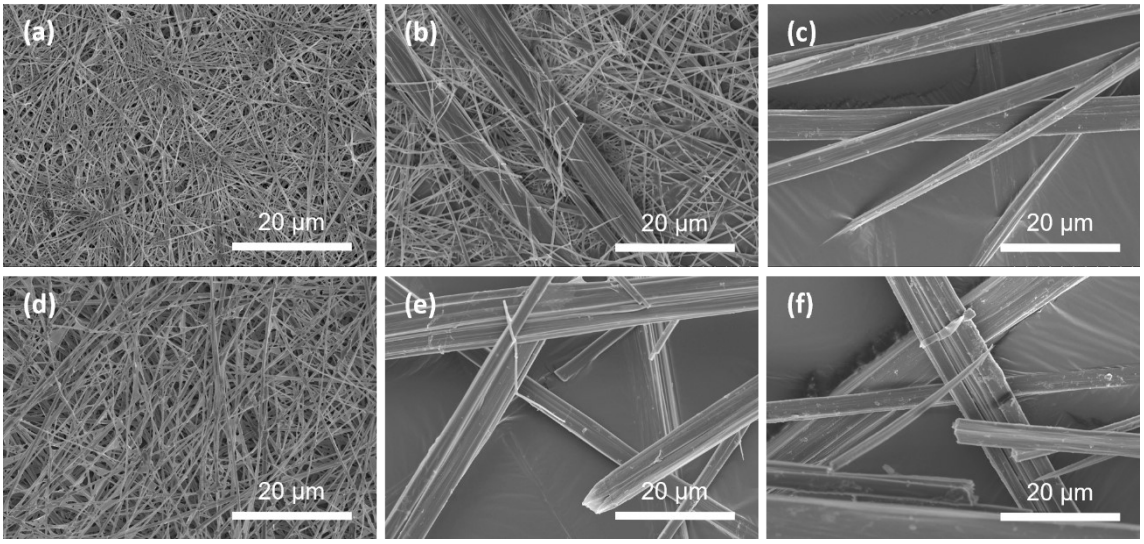

*Figure S19: SEM images of HOF grown in the presence of **Myoglobin**, showing crystals grown upon addition of the (a, b, c) trans- and (d, e, f) cis-K_2.**2** ligand, at HIGH, MEDIUM, and LOW total ligand concentration (L → R).*

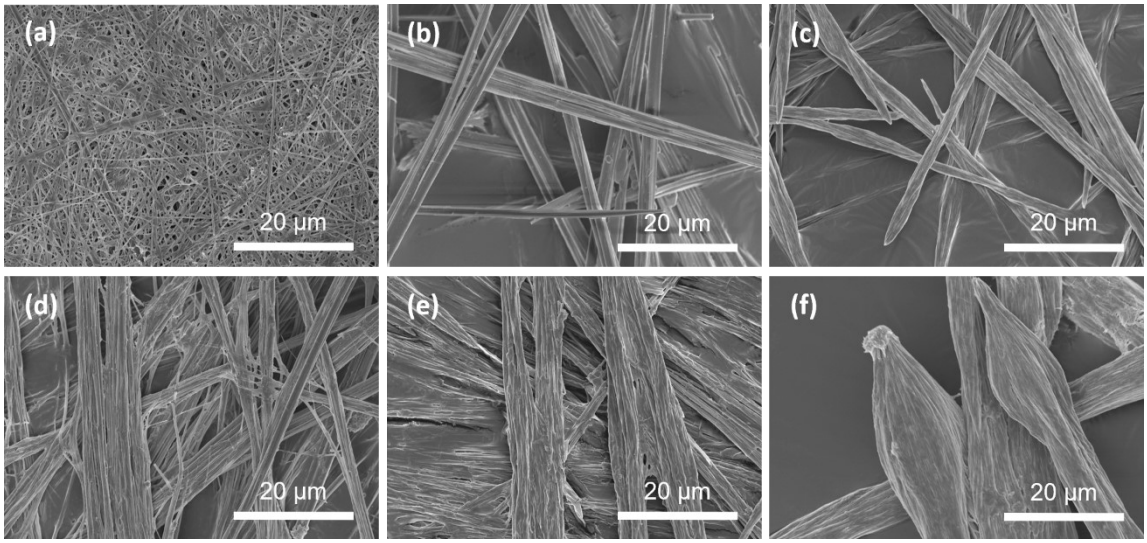

*Figure S20: SEM images of HOF grown in the presence of **Urease**, showing crystals grown upon addition of the (a, b, c) trans- and (d, e, f) cis-K_2.**2** ligand, at HIGH, MEDIUM, and LOW total ligand concentration (L → R).*

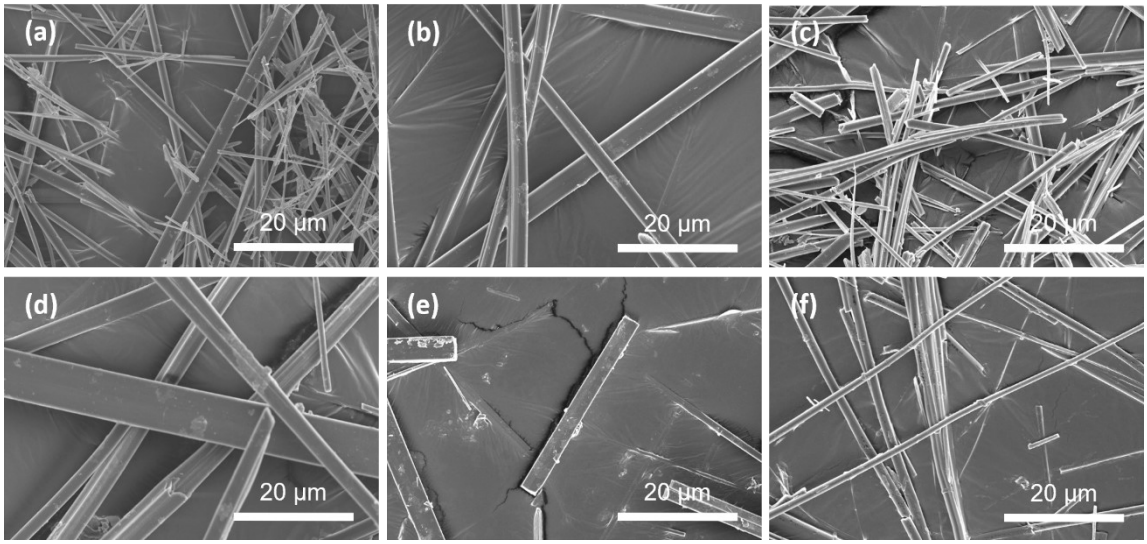

*Figure S21: SEM images of HOF grown in the presence of **Lysozyme**, showing crystals grown upon addition of the (a, b, c) trans- and (d, e, f) cis-K_2.**2** ligand, at HIGH, MEDIUM, and LOW total ligand concentration (L → R).*

S6 Confocal laser scanning microscopy

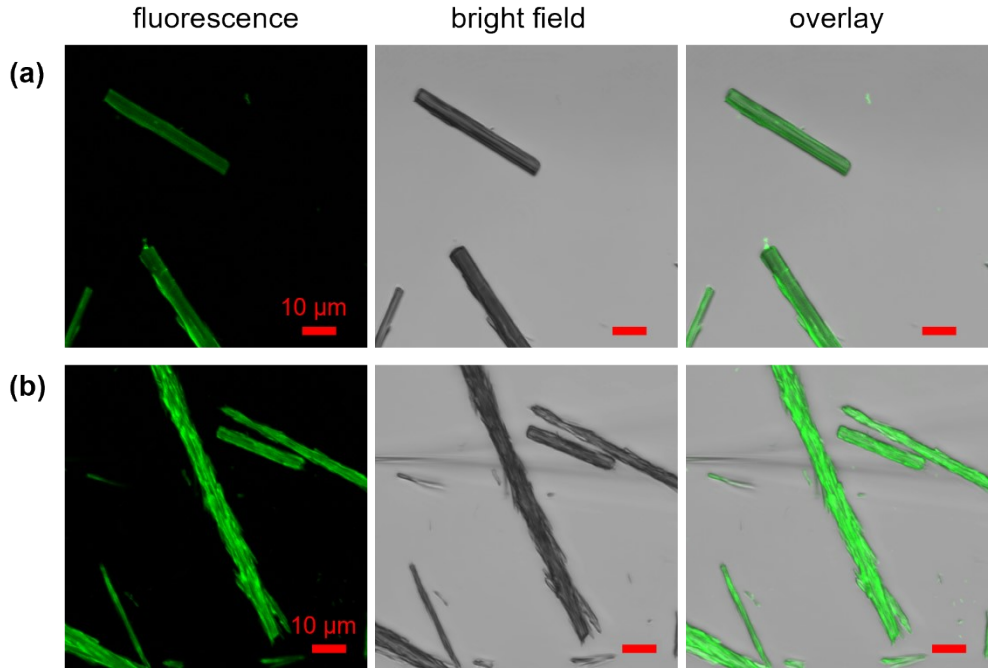

*Figure S22: Confocal laser scanning micrographs showing the fluorescence (left), bright field (centre), and overlay (right) images of **FITC-BSA@HOF** at HIGH ligand concentration. Upon addition of (a) trans-**2** and (b) cis-**2**.*

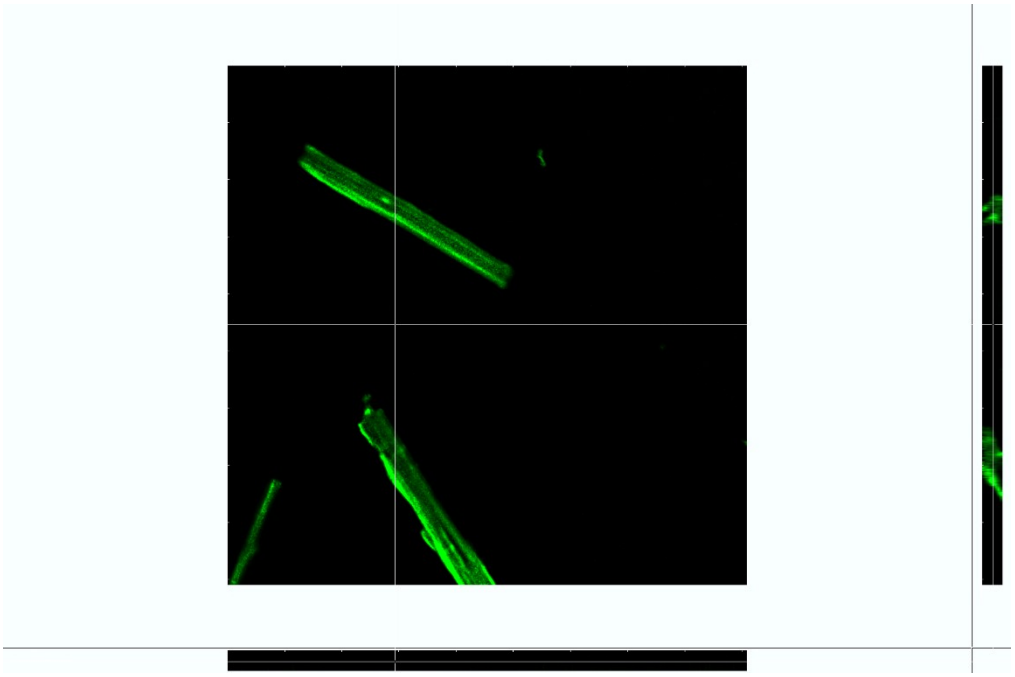

*Figure S23: Confocal laser scanning micrographs from Z-stacks showing **FITC-BSA@HOF** at HIGH ligand concentration upon addition of trans-**2**. Slice shows localisation of FITC-BSA at edges, coating the exterior of the crystals.*

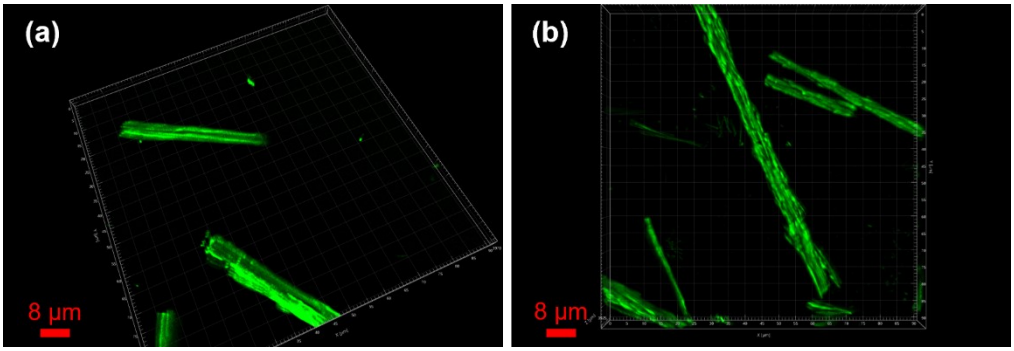

*Figure S24: Confocal laser scanning micrographs Z-stacks showing **FITC-BSA@HOF** at HIGH ligand concentration upon addition of (a) trans-**2** and (b) cis-**2**.*

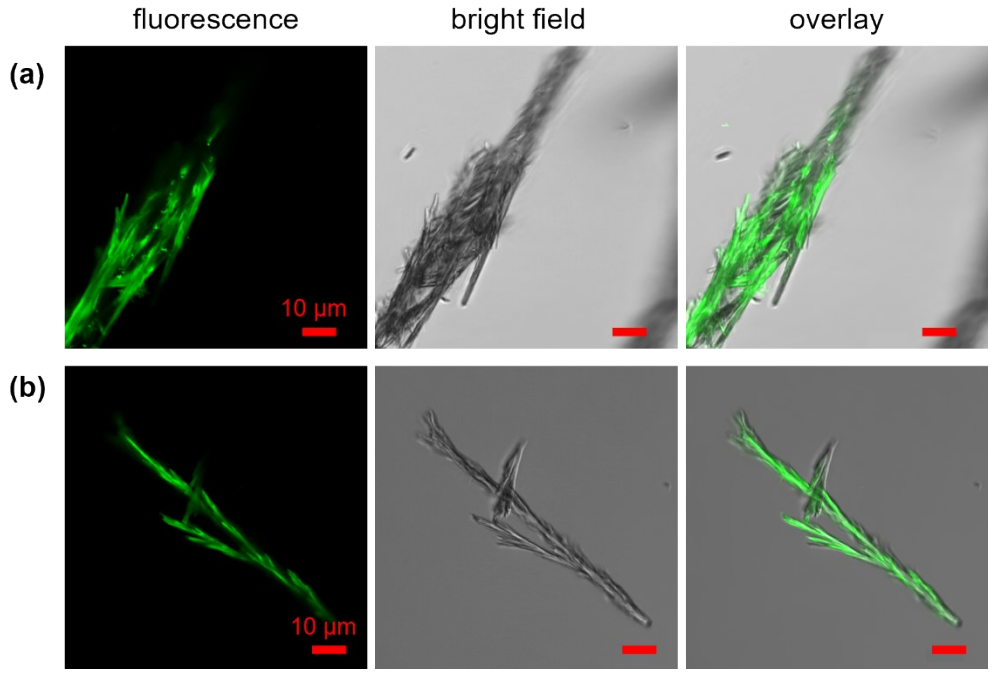

*Figure S25: Confocal laser scanning micrographs showing the fluorescence (left), bright field (centre), and overlay (right) images of **FITC-BSA@HOF** at MEDIUM ligand concentration. Upon addition of (a) trans-**2** and (b) cis-**2**.*

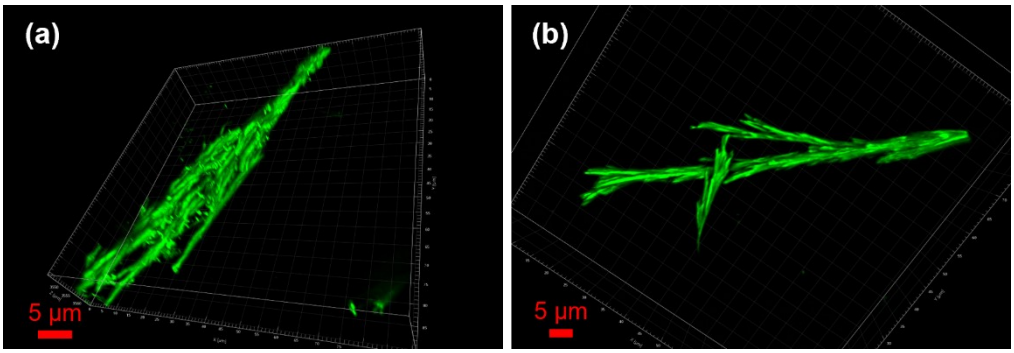

*Figure S26: Confocal laser scanning micrographs Z-stacks showing **FITC-BSA@HOF** at MEDIUM ligand concentration upon addition of (a) trans-**2** and (b) cis-**2**.*

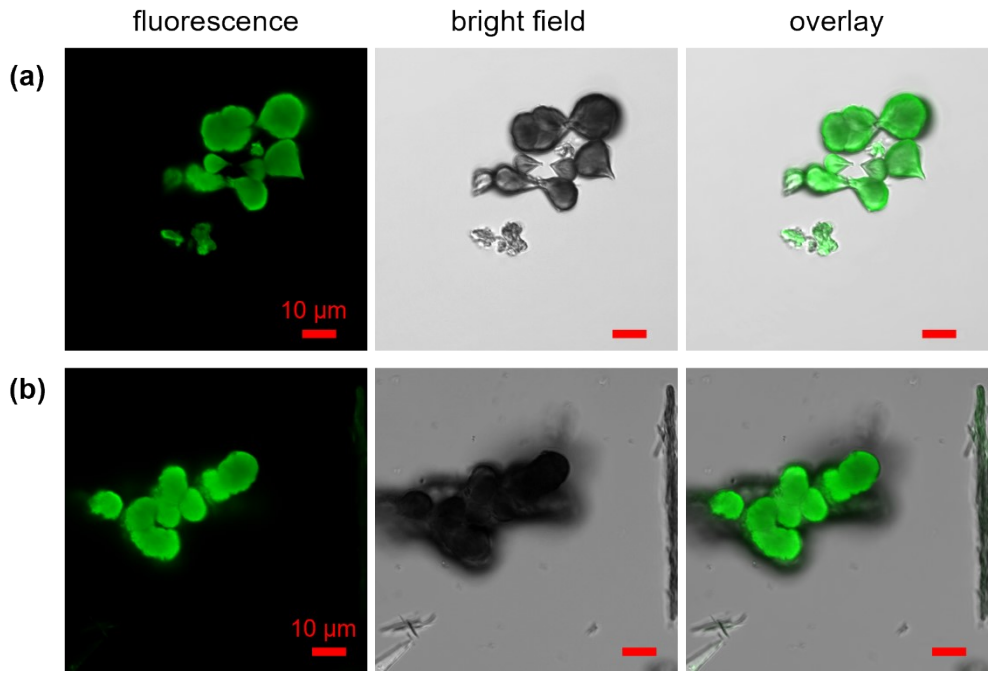

*Figure S27: Confocal laser scanning micrographs showing the fluorescence (left), bright field (centre), and overlay (right) images of **FITC-BSA@HOF** at LOW ligand concentration. Upon addition of (a) trans-**2** and (b) cis-**2**.*

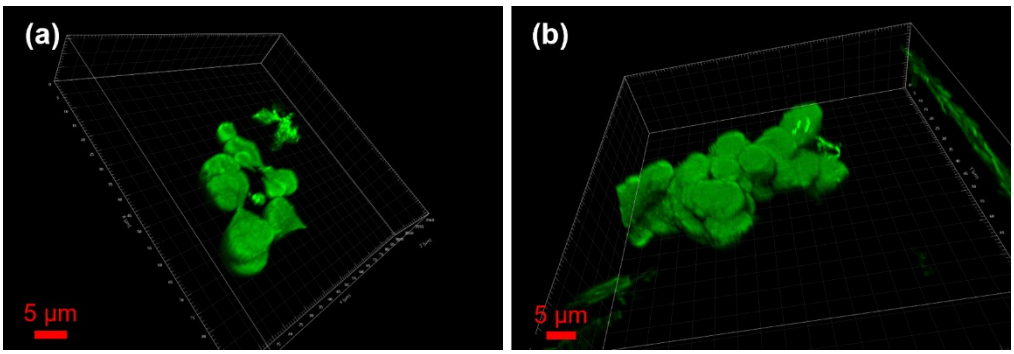

*Figure S28: Confocal laser scanning micrographs Z-stacks showing **FITC-BSA@HOF** at LOW ligand concentration upon addition of (a) trans-**2** and (b) cis-**2**.*

S7 Small Angle X-ray Scattering (SAXS)

Time-resolved SAXS have been collected on the SAXS beamline at the ELETTRA synchrotron light source.[6] We operated at photon energy of 16 keV covering the range of momentum transfer, $q = 4\pi \sin(\theta)/\lambda$, between 0.16 and 6.1 nm^{-1}. We monitored the kinetics of the HOFs nucleation and growth using a commercial stopped flow apparatus SFM-4 (Bio-Logic, Grenoble, France) especially designed for Synchrotron Radiation SAXS investigations.[7] Two independently driven syringes were filled respectively with the K_2.**2** and the **1**.Cl_4/BSA solutions. Two step-motors control the volumes mixed and injected in a 1.5 mm quartz capillary placed in the X-ray beam (the mixing/injection process lasts for a few ms, Figure S32). The volume ratio between the two solutions and their concentration was set to maintain the conditions used for the syntheses in batch that are listed in Table S1.

For each experiment, a total volume of 800 µL was injected. The start of the mixing sequence is triggered by the X-ray data-acquisition system. Images were taken with a time resolution of 100 ms (detector: Pilatus3 1M, Dectris Ltd, Baden, Switzerland; sample to detector distance: 1290 mm, as determined with a silver behenate as calibration sample). The resulting two-dimensional images were radially integrated to obtain a 1D pattern of normalized intensity versus scattering vector q. The Porod Invariant is the integral scattering intensity of an ensemble of particles and is calculated in the q range from 0.16 nm^{-1} to 1.1 nm^{-1}.[8,9] All the experiments were performed at room temperature. The

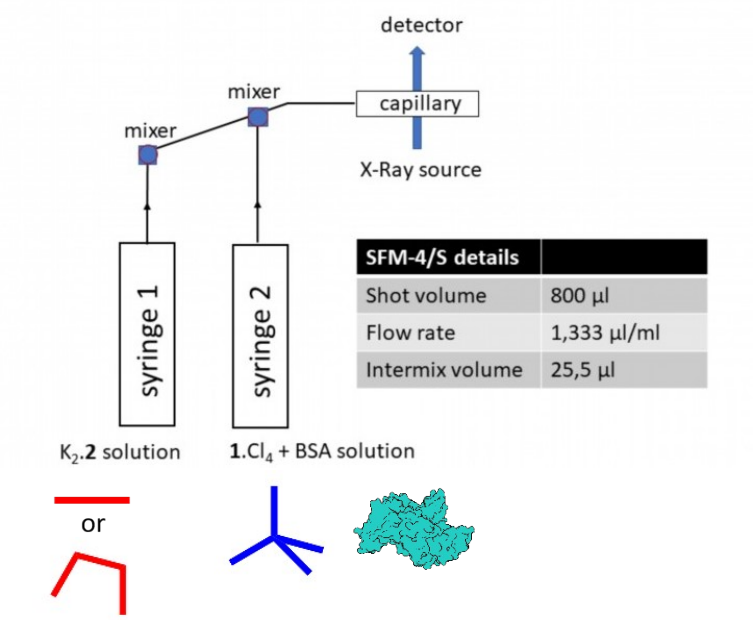

background was collected using Milli-Q water.

Figure S29: Schematic and technical details of the stopped-flow setup.

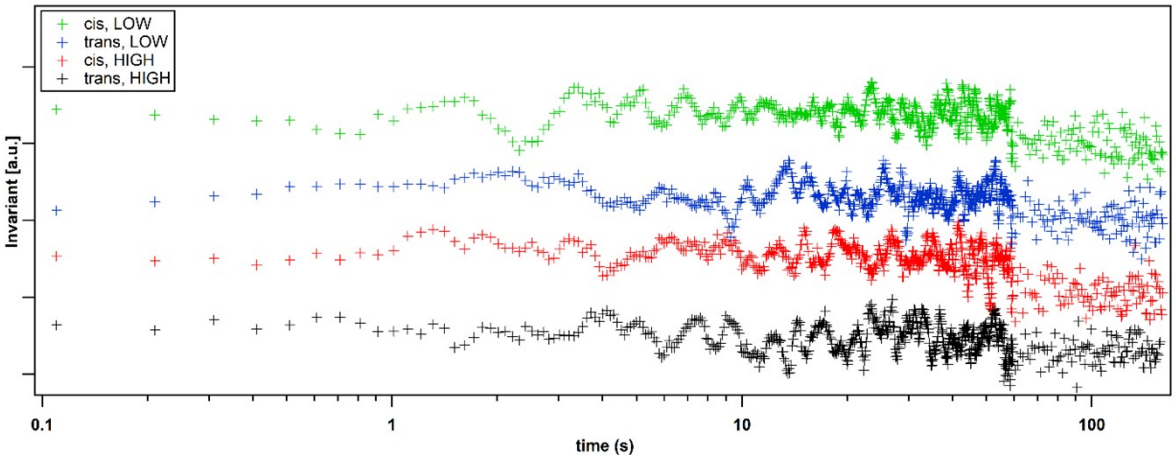

Figure S30: Porod Invariant calculated from the normalized SAXS patterns collected during the time-resolved SAXS study. The data are shifted along the Y-axis for the sake of clarity.

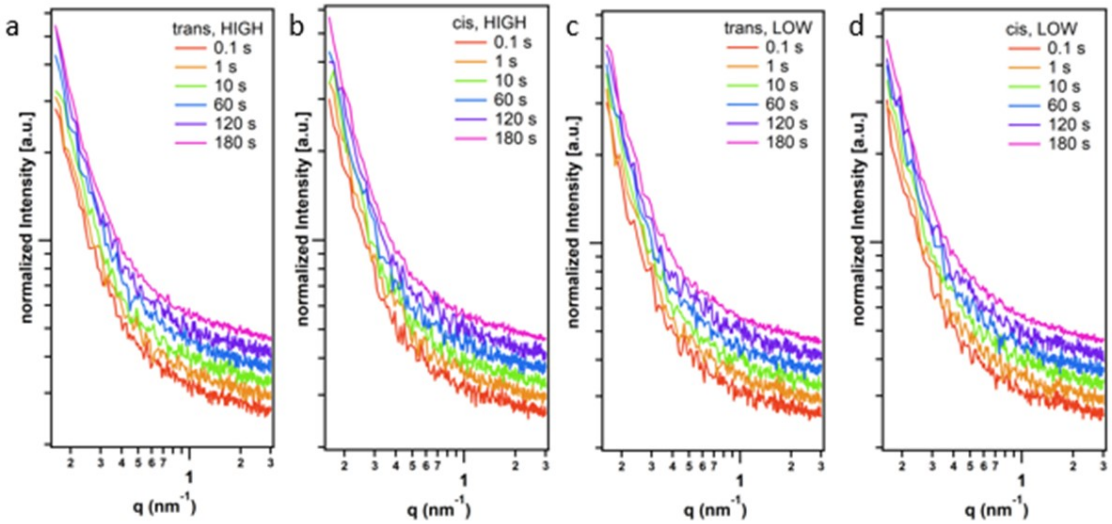

*Figure S31: Time evolution of SAXS patterns from time-resolved SAXS synthesis of the HOF crystals using trans-K_2.**2** with (a) 500 : 1 (HIGH) and (c) 75 : 1 (LOW); and cis-K_2.**2** at (b) 500 : 1 (HIGH) and (d) 75 : 1 (LOW) total ligand concentration. The SAXS patterns were shifted along the Y-axis for the sake of clarity.*

S8 Isothermal titration calorimetry

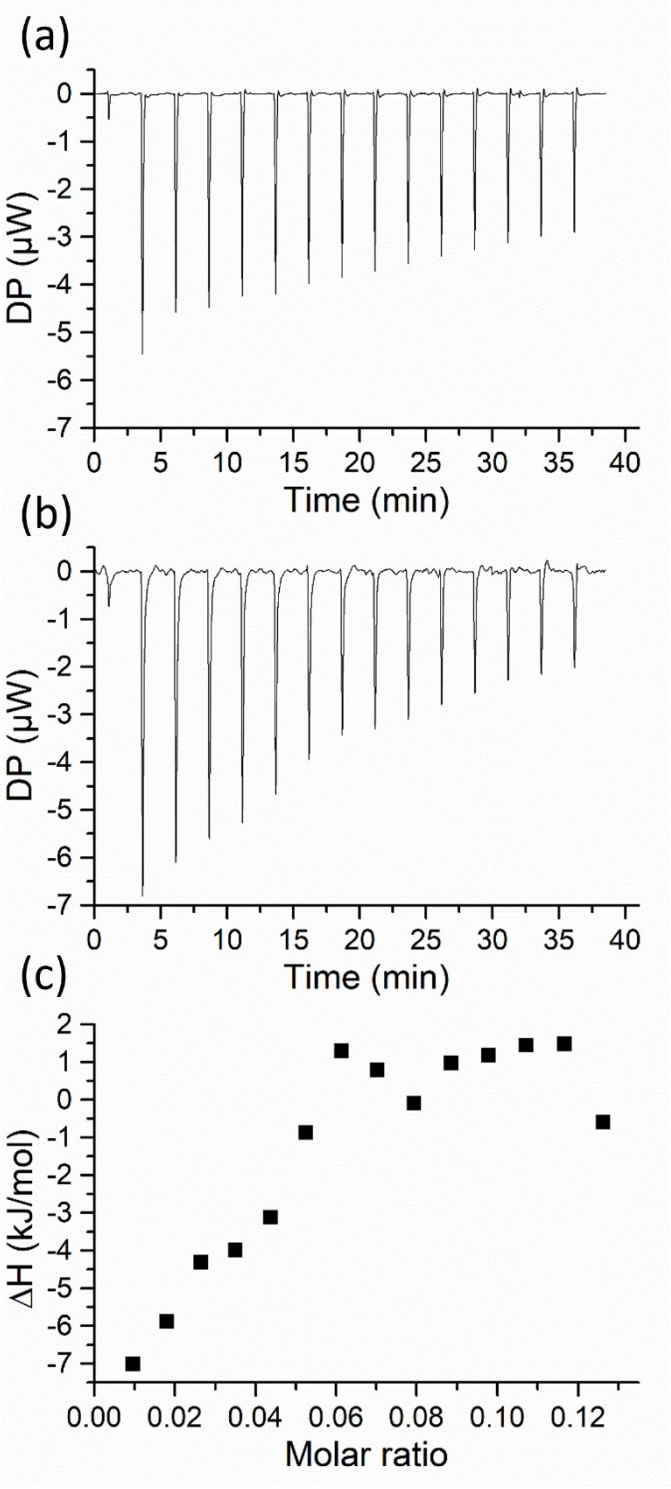

Figure S32: Isothermal titration calorimetry (ITC) at 308 K of (a) ***BSA*** *titrated into 10mM Tris-HCl buffer, pH 7.4, and* ***BSA*** *titrated into HOF showing the experimentally derived curve (b) and the calculated binding isotherm (c). Molar ratio was calculated by comparing the* $mol_{protein}$*:*mol_{HOF} *(*mol_{HOF} *was calculated using the mass of HOF particles in the cell, and the molar mass of one repeating HOF unit i.e.* $\mathbf{1}^{4+}$ *+ (2 x* $\mathbf{2}^{2-}$*)).*

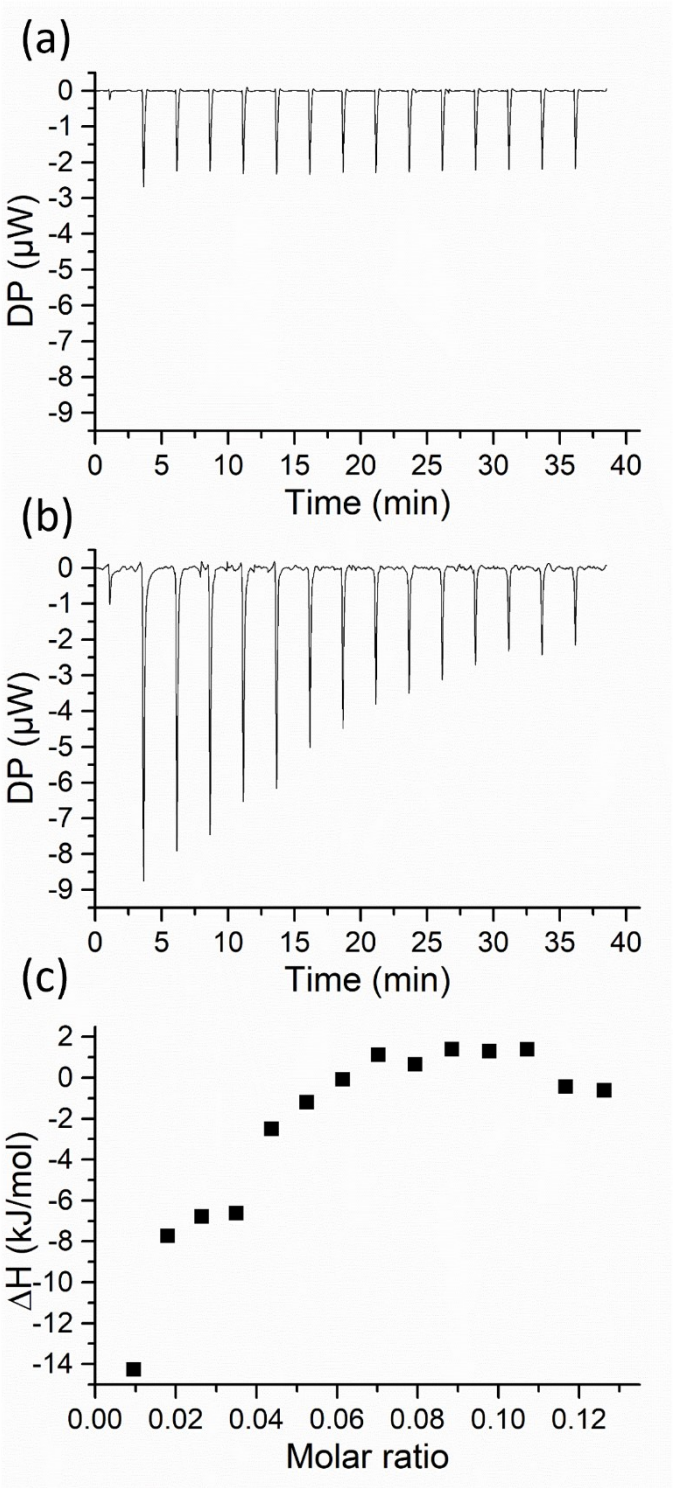

Figure S33: Isothermal titration calorimetry (ITC) at 313 K of (a) ***BSA*** *titrated into 10mM Tris-HCl buffer, pH 7.4, and* ***BSA*** *titrated into HOF showing the experimentally derived curve (b) and the calculated binding isotherm (c). Molar ratio was calculated by comparing the* $mol_{protein}$*:*mol_{HOF} *(*mol_{HOF} *was calculated using the mass of HOF particles in the cell, and the molar mass of one repeating HOF unit i.e.* $\mathbf{1}^{4+}$ *+ (2 x* $\mathbf{2}^{2-}$*)).*

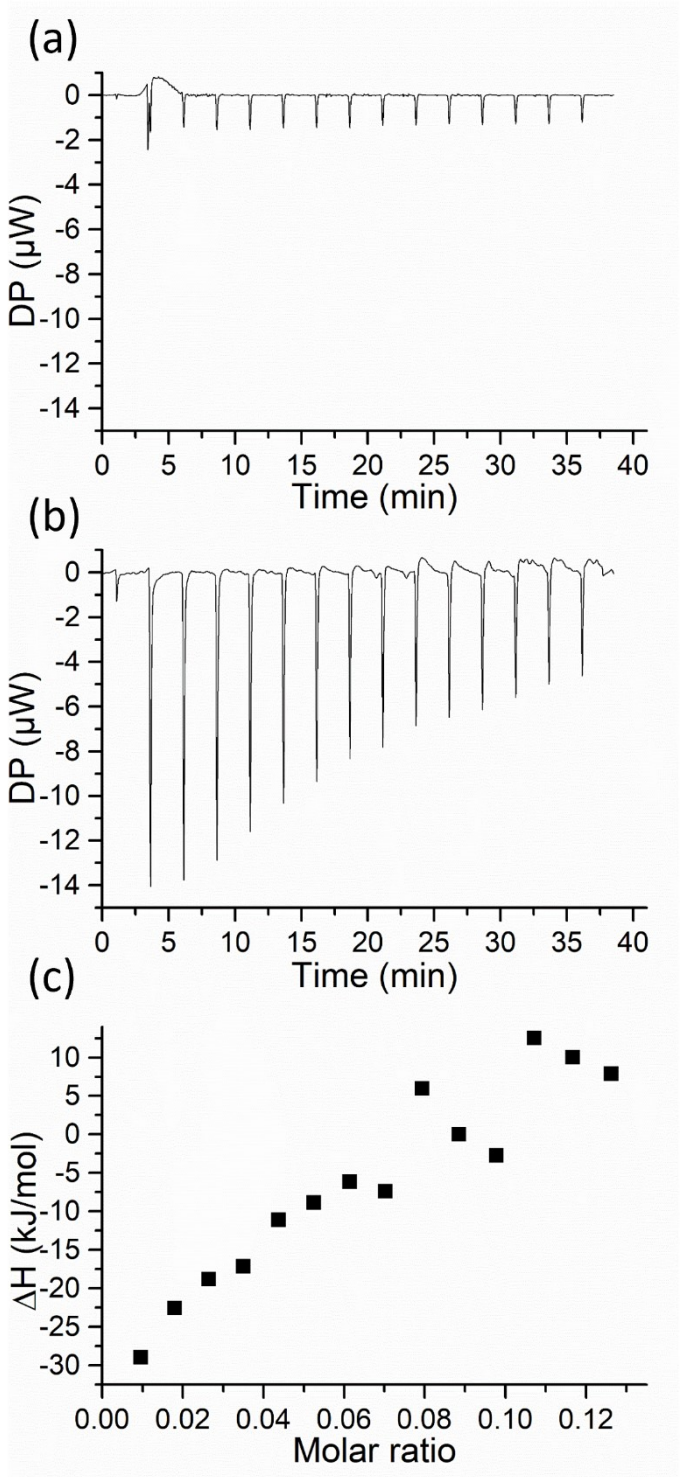

Figure S34: Isothermal titration calorimetry (ITC) at 318 K of (a) ***BSA*** *titrated into 10mM Tris-HCl buffer, pH 7.4, and* ***BSA*** *titrated into HOF showing the experimentally derived curve (b) and the calculated binding isotherm (c). Molar ratio was calculated by comparing the* $mol_{protein}$*:*mol_{HOF} *(*mol_{HOF} *was calculated using the mass of HOF particles in the cell, and the molar mass of one repeating HOF unit i.e.* $\mathbf{1}^{4+}$ *+ (2 x* $\mathbf{2}^{2-}$*)).*

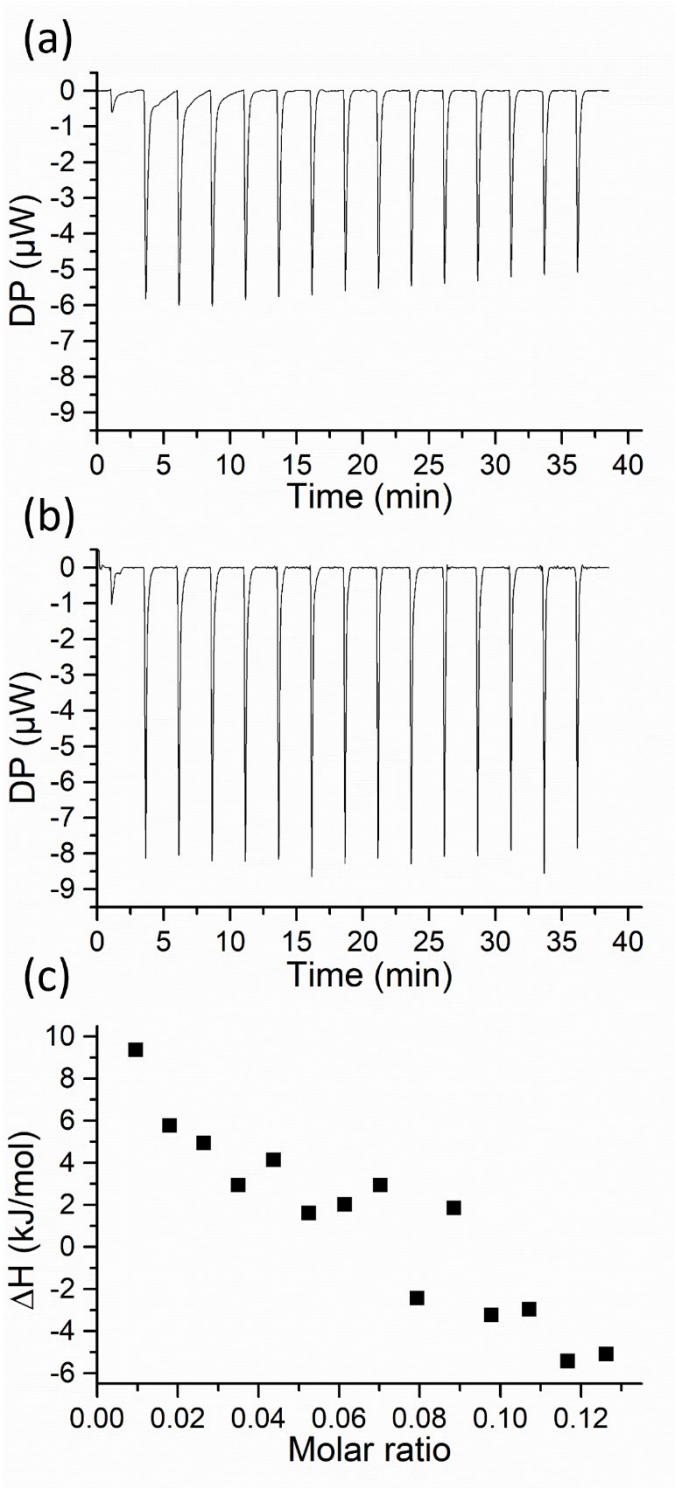

Figure S35: Isothermal titration calorimetry (ITC) at 308 K of (a) ***Lysozyme*** *titrated into 10mM Tris-HCl buffer, pH 7.4, and* ***Lysozyme*** *titrated into HOF showing the experimentally derived curve (b) and the calculated binding isotherm (c). Molar ratio was calculated by comparing the* $mol_{protein}$*:*mol_{HOF} *(*mol_{HOF} *was calculated using the mass of HOF particles in the cell, and the molar mass of one repeating HOF unit i.e.* $\mathbf{1}^{4+}$ *+ (2 x* $\mathbf{2}^{2-}$*)).*

S9 Simulations of surface structure

An automated search of surface structures was employed to discover a model for the surface. Slab models with a Miller index up to 3 were considered with no broken bonds. The approach as implemented in the pymatgen surface module was used.[10,11] Only the (110) surface was found to match these strict conditions. The same approach was applied to produce a similar model of the ZIF-8 (100) surface, for the purpose of comparison. The (100) surface of ZIF-8 is considered to be an important surface expected to enhance catalytic reactions owing to a higher concentration of Lewis acidic sites.[12] Subsequently, these surface models, featuring a minimum slab size of 30 Å and vacuum region of 20 Å, were geometry optimised using density functional theory (DFT). All calculations were carried out using the PBE functional,[13] Goedecker-Teter-Hutter pseudopotential[14] and D3 London dispersion corrections,[15] together with a double-zeta valence (DZVP) basis set for Zn and triple-zeta valence (TZVP) basis sets for all other atoms. A grid cutoff of 800 Ry was employed. The DFT approach used the QUICKSTEP[16] module of the CP2K program package.[17]

These surfaces are not symmetric, each has a dipole present. We observe that the ZIF-8 surface has greater electrostatic potential near the surface owing to Zn sites. The surface of the **1**.Cl_4/K_2.**2** HOF appears to have localised areas of large electrostatic potential due to the carboxylate and amidinium groups but this appears to be lower than ZIF-8. These simulations demonstrate the HOF surface has very different chemistry to that of ZIF-8 where electrostatic are not expected to play an important role in surface-protein interactions.

References

1 M. Morshedi, M. Thomas, A. Tarzia, C. J. Doonan and N. G. White, *Chem. Sci.*, 2017, **8**, 3019–3025.

2 C. C. Epley, M. D. Love and A. J. Morris, *Inorg. Chem.*, 2017, **56**, 13777–13784.

3 N. K. Maddigan, A. Tarzia, D. M. Huang, C. J. Sumby, S. G. Bell, P. Falcaro and C. J. Doonan, *Chem. Sci.*, 2018, **9**, 4217–4223.

4 P. Muang-Non, H. D. Toop, C. J. Doonan and N. G. White, *Chem. Commun.*, 2021, **58**, 306–309.

5 C. F. Macrae, P. R. Edgington, P. McCabe, E. Pidcock, G. P. Shields, R. Taylor, M. Towler and J. van de Streek, *J. Appl. Cryst.*, 2006, **39**, 453–457.

6 H. Amenitsch, M. Rappolt, M. Kriechbaum, H. Mio, P. Laggner and S. Bernstorff, *J. Synchrotron Radiat.*, 1998, **5**, 506–508.

7 I. Grillo, *Curr. Opin. Colloid Interface Sci.*, 2009, **14**, 402–408.

8 O. Glatter, in *Scattering Methods and their Application in Colloid and Interface Science*, ed. O. Glatter, Elsevier, 2018, pp. 97–109.

9 F. Carraro, J. D. Williams, M. Linares-Moreau, C. Parise, W. Liang, H. Amenitsch, C. Doonan, C. O. Kappe and P. Falcaro, *Angew. Chem. Int. Ed.*, 2020, **59**, 8123–8127.

10 R. Tran, Z. Xu, B. Radhakrishnan, D. Winston, W. Sun, K. A. Persson and S. P. Ong, *Sci Data*, 2016, **3**, 160080.

11 W. Sun and G. Ceder, *Surf. Sci.*, 2013, **617**, 53–59.

12 O. M. Linder-Patton, T. J. de Prinse, S. Furukawa, S. G. Bell, K. Sumida, C. J. Doonan and C. J. Sumby, *CrystEngComm,* 2018, **20**, 4926.

13 J. P. Perdew, K. Burke and M. Ernzerhof, *Phys. Rev. Lett.*, 1996, **77**, 3865–3868.

14 S. Goedecker, M. Teter and J. Hutter, *Phys. Rev. B*, 1996, **54**, 1703–1710.

15 S. Grimme, J. Antony, S. Ehrlich and H. Krieg, *J. Chem. Phys.*, 2010, **132**, 154104.

16 J. VandeVondele, M. Krack, F. Mohamed, M. Parrinello, T. Chassaing and J. Hutter, *Comput. Phys. Commun.*, 2005, **167**, 103–128.

17 T. D. Kühne, M. Iannuzzi, M. Del Ben, V. V. Rybkin, P. Seewald, F. Stein, T. Laino, R. Z. Khaliullin, O. Schütt, F. Schiffmann, D. Golze, J. Wilhelm, S. Chulkov, M. H. Bani-Hashemian, V. Weber, U. Borštnik, M. Taillefumier, A. S. Jakobovits, A. Lazzaro, H. Pabst, T. Müller, R. Schade, M. Guidon, S. Andermatt, N. Holmberg, G. K. Schenter, A. Hehn, A. Bussy, F. Belleflamme, G. Tabacchi, A. Glöß, M. Lass, I. Bethune, C. J. Mundy, C. Plessl, M. Watkins, J. VandeVondele, M. Krack and J. Hutter, *J. Chem. Phys.*, 2020, **152**, 194103.